Artvin Çoruh Üniversitesi
Doğal Afetler Uygulama ve Araştırma Merkezi
Doğal Afetler ve Çevre Dergisi

Artvin Çoruh University
Natural Hazards Application and Research Center
Journal of Natural Hazards and Environment

Araştırma Makalesi / Research Article, Doğ Afet Çev Derg, 2024; 10(2): 263-281, DOI: 10.21324/dacd.1400245

Multi-Disaster Hazard Analysis, the Case of Elazığ Province

Fethi Ahmet Canpolat[1,*]

[1]*Fırat University, Faculty of Humanities and Social Sciences, Department of Geography, 23150, Elazığ, Türkiye.*

Abstract

In this study, a comprehensive assessment of disaster hazards in Elazığ province, where the Eastern Anatolian Fault Zone passes through, was conducted. Hazard maps for earthquakes, floods, landslides, rockfalls, avalanches, desertification, and erosion were integrated to create a multi-hazard map. Various methods, such as the Analytic Hierarchy Process (AHP) and machine learning models, including the Random Forest algorithm, were employed to assess the severity and probability of exposure for each hazard type. Independent variables, including VS30, liquefaction potential, Digital Elevation Model (DEM)-derived data, and climatic data, were selected based on relevant literature and the study area. For earthquake and erosion hazards, intuitive models were used due to the absence of a single dependent variable. The desertification map was obtained from the Ministry of Environment, Urban Planning, and Climate Change. The Random Forest model was used for other disaster hazard maps. All hazard maps were combined using a hierarchical approach with the Weighted Overlay tool. The study generated a spatial synthesis and database intended to offer proactive insights into disaster preparedness, optimizing resource allocation, and expediting recovery efforts post-disaster within the Elazığ Province. Its primary objective is to provide assistance to local authorities and emergency response teams. In the province, a significant portion of urban settlements and the majority of rural areas face high earthquake hazards. Floods pose a considerable risk, particularly in low-lying areas downstream of numerous dams scattered across the province, as well as at the confluence points of seasonal riverbeds. The hazard of landslides is high in the rugged areas along the EAF and in steep terrains eroded by rivers. Moreover, rock falls occur more frequently in mountainous areas along the Hazarbaba-Akdağ axis due to erosion and physical dissolution. Erosion and desertification represent significant slow-moving hazards, with erosion intensifying on steep slopes and barren lands, while desertification notably affects Baskil and its surrounding low-lying areas in the western part of the province. Considering multiple hazards, areas with concentrated settlements and economic activities such as Elazığ, Baskil, Kovancılar, Karakoçan, and Behrimaz plains are categorized as very high and high-risk zones.

Keywords

Multi-Disaster Hazard Analysis, Elazığ Province, Earthquake, Flooding, Landslide, Erosion, Rockfall, Avalanche, Desertification

Çoklu Afet Tehlike Analizi, Elazığ İli Örneği

Özet

Bu çalışmada, Doğu Anadolu Fay Zonu'nun geçtiği Elazığ ilinde, afet tehlikelerinin çoklu değerlendirmesi yapılmıştır. Çoklu afet tehlike haritası oluşturmak için deprem, sel, heyelan, kaya düşmesi, çığ, çölleşme ve erozyona ilişkin tehlike haritaları kullanılmıştır. Analitik Hiyerarşi Süreci (AHP) ve Rastgele Orman (RO) algoritması da dahil olmak üzere çeşitli yöntemler, her bir tehlike türü için maruziyetin ciddiyetini ve olasılığını değerlendirmek amacıyla kullanılmıştır. Bağımsız değişkenler, ilgili literatüre ve çalışma alanına dayalı olarak seçilmiş ve sonuçta VS30, sıvılaşma potansiyeli, sayısal yükselti modelinden türetilmiş veriler ve iklim verileri de dahil olmak üzere 30 değişken elde edilmiştir. Deprem ve erozyon tehlikeleri için bağımlı değişken bulunmamasından dolayı sezgisel modeller kullanılmıştır. Çölleşme haritası, Çevre Şehircilik ve İklim Değişikliği Bakanlığından alınmıştır. Tüm tehlike haritaları, Coğrafi Bilgi Sistemleri yazılımındaki ağırlıklandırılmış katman aracıyla hiyerarşik bir yaklaşım kullanılarak birleştirilmiştir. Araştırma ile Elâzığ ilinde afetlere karşı hazırlıklı olmayı sağlama, kaynakları etkin bir şekilde kullanma ve afet sonrası toparlanma sürecini hızlandırma çalışmaları için öngörü sağlayabilecek mekânsal bir sentez ve veri tabanı oluşturulmuştur. Böylece yerel yönetimlere ve acil müdahale ekiplerine yardımcı olması amaçlanmıştır. Deprem açısından ildeki kentsel yerleşmelerin önemli bir bölümü, kırsal yerleşmelerin ise çoğunluğu yüksek tehlike altındadır. Sel ve taşkın tehlikesi başta depresyon sahaları olmak üzere, il genelinde çok sayıda bulunan barajların mansap kesimlerinde ve mevsimlik akarsu yataklarının birleştiği yerlerde yüksektir. Heyelan tehlikesi, DAF boyunca uzanan engebeli alanlar ile akarsular tarafından aşındırılan yüksek eğimli arazilerde fazladır. Kaya düşmeleri özellikle Hazarbaba-Akdağ ekseni boyunca yer alan dağlık arazilerde, erozyona ve fiziksel çözülmeye bağlı olarak artmaktadır. Erozyon ve çölleşme il genelindeki en önemli yavaş ilerleyen tehlikelerdendir. Erozyon yüksek eğimli ve çıplak arazilerde artarken, çölleşme özellikle ilin batısında düşük yükseltiye sahip Baskil ve çevresinde etkisini göstermektedir. Çoklu tehlike açısından; Elazığ, Baskil, Kovancılar, Karakoçan ve Behrimaz ovaları gibi yerleşme ve iktisadi faaliyetlerin yoğunlaştığı alanlar çok yüksek ve yüksek tehlikeli alanlar arasında yer almaktadır.

Anahtar Sözcükler

Çoklu Afet Tehlike Analizi, Elazığ İli, Deprem, Sel ve Taşkın, Heyelan, Erozyon, Kaya Düşmesi, Çığ, Çölleşme

* Corresponding Author: Tel: +90 (424) 6073516 Faks: +90 (424) 2330062
E-mail: facanpolat@firat.edu.tr (Canpolat FA)

Gönderim Tarihi / Received : 04/12/2023
Kabul Tarihi / Accepted : 15/02/2024

1. Introduction

While the number of fatalities from disasters worldwide is decreasing, the number of disasters is increasing (United Nations Office for Disaster Risk Reduction, 2022). As a result, the risk of loss of life and property persists. Various factors such as urbanization, underdevelopment, desertification, climate change, population growth, migration, and conflict are major contributors to the increasing incidence of disasters. Türkiye is a country with a high vulnerability to disaster risks. This vulnerability is mainly due to its location along one of the most active tectonic belts in the world, which leads to earthquakes, the increasing influence of seasonal anomalies in the temperate zone, and inappropriate urban development, which leads to floods, droughts, and desertification. In addition, the rugged topography, combined with the tectonic structure and climatic characteristics, plays a crucial role in mass movements, while forest fires are increasing due to human negligence and deliberate ignition, exacerbated by summer heat.

The primary objective of risk assessment is to measure the likelihood of human and economic losses resulting from an event, defined as a 'hazardous incident', due to the occurrence of such an event (UNEP, 2004). In the ecumenical domain of the world, there are generally risks associated with multiple disasters in any given location (Jha et al., 2013; Hutter, 2017; United Nations Office for Disaster Risk Reduction, 2022). However, disaster risk analyses typically focus on a single type of hazard, such as earthquakes, landslides or floods. In most places, there is exposure to hazards triggered by multiple interacting, incremental impacts occurring simultaneously. In addition to single-hazard assessments, there has been a growing interest in recent years in conducting multihazard assessments, which are more essential but involve a challenging and complex process. This is because it requires the selection of appropriate and accurate independent variables and models for the individual production of each hazard map, which requires effective management of information processes (Aksha et al., 2020; Marzocchi et al., 2012).

Assessments related to multiple disasters can be classified into different categories, such as multi-disaster hazard analyses, integrated disaster hazard analyses and hybrid disaster hazard analyses. Multi-disaster hazard analyses, which emerged in the 1990s, generally involve the simultaneous analysis of multiple disaster hazards by a single scientific discipline (United Nations Department of Public Information, 1994; Kappes et al., 2012; Aksha et al., 2020). Integrated or comprehensive disaster hazard/risk analyses, initiated in the 2000s under the leadership of the United Nations, are another approach that brings together different disciplines and perspectives to ensure a comprehensive understanding of risks. The term 'integrated' also implies an assessment of how disasters affect each other, recognising that disasters are complex phenomena that require a holistic approach for effective analysis and management. However, there are many criticisms of the lack of a multidisciplinary approach in the majority of studies using this approach (Gill & Malamud, 2014; Gall et al., 2015; Sutley et al., 2017). Finally, hybrid disaster risk analysis, which emerged in the 2010s, is an approach that combines comprehensive quantitative and qualitative data to identify potential hazards and vulnerabilities and assess their impacts on communities and infrastructure. The resilience-focused hybrid disaster risk analysis process involves various steps, including hazard identification, vulnerability assessment, risk characterisation and risk communication (Ekmekcioğlu et al., 2021).

This study presents a multi-disaster hazard risk assessment model applied to the province of Elazığ, which is located along the East Anatolian Fault Zone. The study area is highly vulnerable to various disasters, mainly earthquakes, but also landslides, floods, rockfalls, avalanches, desertification and erosion. The North and East Anatolian Faults, which are among the most seismically active zones in Türkiye, result from the westward movement of Anatolia. The East Anatolian Fault, which starts at Bingöl Karlıova and passes through Elazığ, Malatya, Adıyaman and Kahramanmaraş, has a high potential for earthquake generation. The losses associated with the Elazığ earthquake in 2010 and 2020 and the Kahramanmaraş earthquake in 2023 are indicative of this high seismic risk.

2. Study Area

Elazığ Province is located in the southeastern part of Türkiye. It covers an area of 9,327 square kilometers and lies between 40°22' and 38°20' east longitude and 38°14' and 39°11' north latitude. The province is bordered by Bingöl to the east, Tunceli, separated by the Keban Dam Lake, to the north, Malatya, bordered by the Karakaya Dam Lake, to the west and southwest, and Diyarbakır to the south (Figure 1).

In 2007, when the address-based population registration system was launched, the total population of the province was around 541,000, with 151,000 living in rural areas and 390,000 in urban areas. By 2022, the population had increased to 591,000, with 131,000 in rural areas and 460,000 in urban areas (Turkish Statistical Institute, 2023). Settlement areas in the province expanded significantly from about 8,000 hectares in 2000 to 29,000 hectares in 2022, a 3.6-fold increase. The location of housing, particularly in rural areas, has become more dispersed. Of the province's total land area, approximately 47,600 hectares are designated as agricultural land, 16,130 hectares as forest land, and the remaining land consists of low vegetation density areas and inland waters.

The expansion of settlement and agricultural areas in the province has increased the potential for natural events to turn into disasters. Due to the influence of the East Anatolian Fault (DAF), earthquakes are a significant hazard in the districts of Sivrice, Palu and Karakoçan.

Landslides are common in Palu, Karakoçan and Arıcak districts, while floods and inundations are particularly common in Palu, Karakoçan, Arıcak, Sivrice, Baskil and Maden districts. Rockfall is a significant hazard in Palu and Arıcak districts, and in Karakoçan and Baskil districts. According to the Disaster Risk Reduction Report prepared by the Disaster and Emergency Management Presidency (AFAD), 32 landslides, 23 rock falls, 10 avalanches and 24 multiple disasters occurred in Elazığ between 1960 and 2019. In addition, the province experienced 88 destructive earthquake events between 1900 and 2021 (Elazığ Provincial Directorate of Disaster and Emergency, 2021). In recent years, slowly developing disasters such as erosion and desertification have expanded their impact and area in the province.

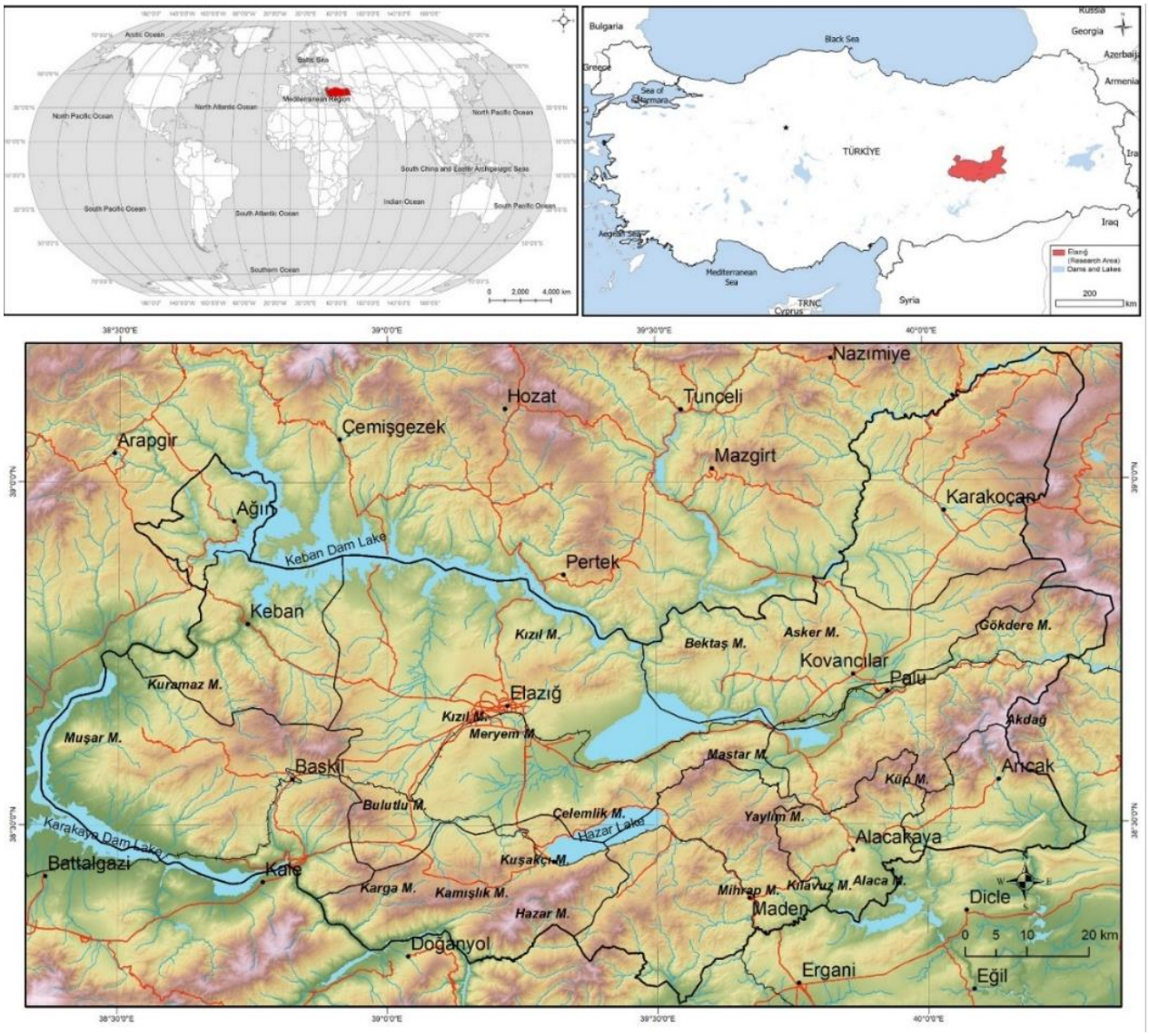

Figure 1: Location map of Elazığ province

3. Materials and Methods

3.1. Data Sources

In this study, earthquake, flood, landslide, rockfall, avalanche, desertification and erosion hazards were assessed as part of the multi-hazard hazard analysis. Floods and inundations were obtained from the 100-year flood data of the National Water Information System, landslides from the Geoscience Information System of the MTA, rockfalls and avalanches from the inventory of the AFAD (Disaster and Emergency Management Authority) based on date and location information. Hazard maps of these disasters were generated using a random forest model. Unlike other disasters, earthquake is not a disaster that can be classified using a dependent variable, so it is treated using a hierarchical approach. Analytical hierarchy process was used in this study. The desertification hazard map was obtained from the Ministry of Environment, Urbanisation and Climate Change.

In order to create separate hazard maps for each disaster, conditioning factors were selected based on the literature. The independent variables used in the models and their justification are as follows:

x1. Lithology: Another important parameter in determining earthquake hazards is the control of seismic wave propagation by lithology and the environment (Yanis & Furumoto, 2019). The lithology data were obtained by digitizing MTA's 1:500,000 scale geological maps of Sivas and Erzurum (Bilgiç, 2002; Tarhan, 2002). In the province, 39 distinct geological and lithological combinations have been assessed based on literature and categorized into 5 hierarchical classes. This factor, crucial for landslides, floods, inundations, and rockfalls, has been transformed into continuous/numerical data using the frequency-density method and subsequently integrated into the models (Figure 2).

x2. Development of the Settlements: One of the most decisive factors in the destruction caused by the earthquake is the quality of the buildings in the settlement (Zengin & Aydin, 2023). In Türkiye, the construction of relatively more earthquake-resistant buildings has increased, particularly after the 1999 Düzce earthquake, due to the implementation of earthquake regulations. Recent earthquakes in the province have raised awareness of this issue. As a result, it has been observed that newly constructed buildings are generally more resistant to earthquakes, both in terms of age and construction methods. To obtain this parameter, historical development data of settlements between 1985 and 2015, obtained from Landsat imagery, were combined with the settlement layer in the land use data obtained from Esri's Sentinel 2 to obtain historical development data between 1985 and 2023 (World Settlement Footprint, 2023; Environmental Systems Research Institute, 2023).

x3. VS30: This variable, like shear wave velocity, is used to determine rock classification based on earthquake seismic resistance. However, it can only determine the amplification of earthquake waves for rock layers up to a depth of 30 meters (Rusydi, Effendi & Rahmawati, 2017). In general, a higher VS30 value suggests that the soil is less prone to shaking during an earthquake, implying that structures may be more resistant to seismic effects. This data was obtained from the Vs30 map published by the USGS and produced at a global scale with a resolution of 827.5 meters (Heath et al., 2020). The 'topo to raster' tool in the GIS software was used to reduce the resolution to 30 meters.

x4. Liquefaction: Due to the strong impact of earthquakes, the pore water pressure in the soil increases, causing the granular materials in the soil to transition from solid to liquid, significantly disrupting the stability of structures and leading to an increase in earthquake intensity (Zhou et al., 2022). To determine earthquake hazard, this variable was used by resampling the global liquefaction hazard map produced by Koks et al., (2019). The same method was used in VS30 to change the resolution.

x5. Slope: In areas with steep slopes, the potential for the development of floods and mass movements is high due to the faster flow of rain or snowmelt water. Additionally, areas with steep slopes may have less vegetation, increasing the risk of soil erosion. In contrast, in areas with lower slopes, surface runoff is slower, and there is a higher level of infiltration. Floods occur in small basins with steep slopes, while inundations occur in flat or near-flat areas (Toprak and Canpolat, 2022). As this data is derived from the digital elevation model (DEM), there is no need for changes in resolution.

x6. Elevation: Elevation determines environmental control and forms the basis for spatial variation in hydrological conditions and slope stability in a given region. Therefore, the importance of elevation in hydrological and slope stability studies cannot be underestimated (Efiong et al., 2021). The low correlation between elevation and earthquakes, as indicated by the results of the correlation analysis, is related to the evaluation based on epicentre data. The primary relationship between earthquakes and elevated areas is due to the fact that higher areas experience less impact on the ground. In other words, areas that are geologically safer are also places where earthquake intensity decreases, regardless of the magnitude of the earthquake. There is therefore a strong negative correlation. The study used the ~30-meter resolution SRTM digital elevation model (Earth Resources Observation and Science Center, 2017). As some of the independent variables were derived from this dataset, the resolution of all variables was adjusted to match this data.

x7. Distance to Faults: Distance to faults is a fundamental determinant of where earthquakes occur. This distance also plays a triggering role in mass movements (Korup et al., 2007). Active fault data were obtained by digitizing the Elazığ sheet of MTA's 1:250000 scale Türkiye Active Fault Map Series (Duman et al., 2012). In the province, the faults that cause the most earthquakes are the East Anatolian Fault (DAF) and its extensions, which run in the NE-SW direction.

x8. Distance to Epicenters & x9. Epicenter Density: The hypocentre is the underground location where the energy initially stored along a locked fault is first released. The epicentre, on the other hand, is the surface location closest to the hypocentre (Harff et al., 2016). Earthquake epicenters and magnitudes were obtained from AFAD and Kandilli Observatory online earthquake catalogues (Disaster and Emergency Management Presidency, 2023; Boğaziçi Üniversitesi Kandilli Rasathanesi ve Deprem Araştırma Enstitüsü, 2023). The earthquake hazard assessment used the density of magnitude 4 or greater epicentres from 1900 to the present and the distance to these epicentres across the province.

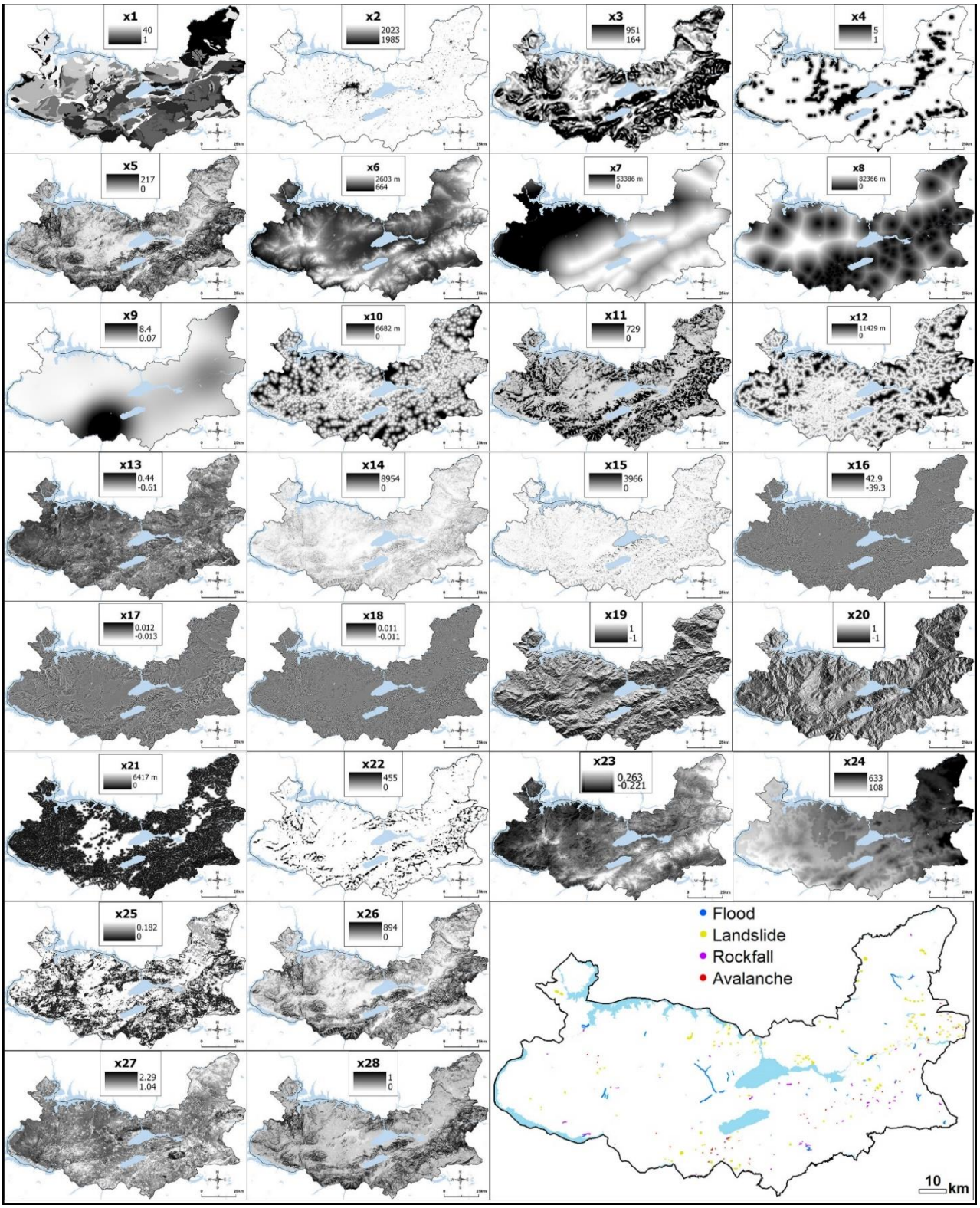

Figure 2: Independent and dependent variables used in the production of disaster hazard maps

x10. Distance to Settlements: This parameter plays a crucial role in flood disasters, mainly due to the impermeable surfaces formed by construction activities. To generate the data, Euclidean distance analysis was employed on the settlement layer extracted from Google Dynamic World V1 data (Brown et al., 2022).

x11. Distance to Streams: Distance from rivers is a critical factor in predicting floods and mass movements. Intensive rainfall areas adjacent to rivers intensify flood events due to water accumulation (Das 2019). Disruption of slope stability due to riverbank erosion can trigger mass movements (Corominas et al., 2003).

This data was obtained using the digital elevation model and hydrography tools in the SAGA-GIS software. Both perennial and seasonal rivers were used to assess distance to rivers and all were considered important.

x12. Distance to Roads: The distance to roads plays an important role in mass movements due to its impact on slope stability (Schicker & Moon, 2012). In addition, the effect of roads on natural drainage systems has an impact on flood activity (Rogelis, 2015). This data has been extracted from the Open Street Maps data catalogue (GEOFABRIK, 2023).

x13. NDBI: Settlement areas serve as impervious surfaces and play an important role in flood disasters (Li et al., 2023). It was used because of its significant correlation with various disasters, including floods. This data, similar to the NDVI 2023 images from Sentinel 2, was produced on the Earth Engine platform and its resolution modified in the same way.

x14. Stream Transportation Index (STI): STI, another flood conditioning factor that defines the movement of sediments due to water flow. Erosion and deposition processes are characterized using STI (Tehrany et al., 2019). This factor, derived from DEM, has also been used for rockfall and landslide disasters, in addition to floods and inundations.

x15. Stream Power Index (SPI): This data has been obtained with the aid of the digital elevation model and hydrography tools in SAGA GIS. The stream power index is often used to classify floods and inundations. In this index, areas with values less than 6 are considered sensitive to floods, while areas with values greater than 6 are considered sensitive to stream floods (Khosravi et al., 2016).

x16. Topographic Position Index (TPI): TPI, another data produced by DEM, shows how high or low the height of a pixel is compared to the heights of the surrounding pixels. The combination of TPI at both small and large scales allows the differentiation of landforms (Weiss, 2001). These data, which include slope and elevation information, have been found to be negatively to moderately correlated with floods and positively correlated with avalanches.

x17., x18. Profile Curvature and Plan Curvature: This variable, which expresses the curvature of the terrain, is a measure of how much a surface deviates from being perfectly flat. Profile curvature measures the acceleration/deceleration of flow, while plan curvature is related to the convergence/divergence of flow along the surface (Efiong et al., 2021). In terms of curvilinearity, convex surfaces can lead to increased erosion and trigger floods and inundations (Sahana and Patel, 2019).

x19., x20. Notherness and Easterness: As the aspect variable is categorical, it must be transformed into a continuous variable, either using dummy variables or the frequency density method, in order to be included in models. Alternatively, the effect of aspect is sometimes exploited by taking the sine of the aspect angle for east-facing or non-east-facing aspects, referred to as 'easterness' (Tonini et al., 2020). Northerness, which corresponds to the cosine of the aspect angle, is included in models for similar purposes as it influences variations in factors such as temperature, snowmelt and vegetation on sun-exposed slopes.

x21. Distance to Ridges: This variable, along with the next two variables, was derived from the DEM using the terrain analysis tools in SAGA GIS. Proximity to ridges increases sensitivity to mass movements (Yeon et al., 2010). While there is a weak negative correlation between this factor and landslide and rockfall disasters, a strong negative correlation is observed with avalanche catastrophes. The avalanche hazard model incorporated the distance to ridges of 1700 meters and above, taking into account the distribution of avalanche catastrophes.

x22. Ridge of Heights: This variable, which identifies high areas and peaks in the terrain, shows a moderate positive correlation with avalanche and rockfall catastrophes. The factor is obtained using the formula developed by Rodriguez and colleagues (2002). Considering the relationship between altitude and these two disasters, identifying areas that are higher than their surroundings has improved the accuracy of the model predictions.

x23. Normalized Difference Snow Index (NDSI): To effectively identify areas with snow cover, remote sensing techniques employ both the visible green spectral band (G) and the shortwave infrared (SWIR) bands of the electromagnetic spectrum. To do this, the formula NDSI=(Green-SWIR)/(Green+SWIR) is used (Abdulkadhim, 2019). To generate the Normalized Difference Snow Index (NDSI) image, snow cover data was compiled over a multi-year period from 2010 to 2024, and the average values were calculated. However, due to the similarity in spectral signatures between snow-covered areas and water bodies, the NDSI values for wetland regions could not be reliably distinguished. As a result, the wetland areas were identified and their NDSI values were reassigned to 0 to avoid potential misclassification with snow cover.

x24. Rainfall-runoff (R) Factor: Rainfall erosivity differs from rainfall in that it includes factors such as rainfall volume, duration, intensity and size. This factor is derived from the open-access rainfall erosion database at 1 km resolution based on global hourly rainfall records by Panagos and colleagues (Panagos et al., 2023). To achieve a 30-meter resolution, the raster data was converted to point data, and the resulting dataset was recorded with spatial interpolation at a resolution of 31 meters.

x25. Soil Erodibility (K) Factor: This factor, used to determine erodibility based on soil type, is obtained by calculating the structural properties of soil types according to the formula developed by Wischmeier and Smith (1958). The data, comprising physical and chemical properties, was acquired from a recent global soil database as raster files (Poggio et al. 2021). After calculations, the coefficients were converted to point data and subsequently spatially interpolated to 31 meters. K-factor values for seven soil types in the province ranged from 0.169 to 0.182.

x26. Length of Slope (LS) Factor: The L factor describes the effect of slope length, while the S factor characterizes the effect of slope steepness.

Among the six input layers of the Universal Soil Loss Equation (USLE) model, the most commonly used model for erosion risk assessment, these factors have a significant effect on soil loss (Panagos et al., 2015). This parameter was derived from the digital elevation model using the LS-Factor (one step) tool in the SAGAGIS software.

x27. Land Cover Management (C) Factor: The C-factor represents the effect of cropping and management practices on the erosion rate. To obtain this data, the Normalized Difference Vegetation Index (NDVI) was calculated from Landsat 8 images taken in 2023 at a 30-meter resolution. The formula $C=e^{((-2.5\times NDVI)\div(1-NDVI))}$, developed by Knijff et al. was then applied to the obtained data (Knijff et al., 2000).

x28. Support Practice (P) Factor: The P-factor is a parameter that influences erosivity based on the combination of land use types and slope. On the map, a value of 0 indicates the highest effectiveness of protective measures, while a value of 1 indicates the absence of any supportive or preventive measures (Wischmeier & Smith, 1958). The Supporting Practices Factor (P) for Elazığ Province was calculated according to Shin (1999) by land use type and slope in a range of values from 0.003 to 1.00.

Beyond these parameters, Microsoft's 2019 building footprints were employed to identify residential areas at risk. The dataset revealed a total of 142.046 buildings in the province (World Settlement Footprint, 2023). For the identification of agricultural areas at risk, agricultural zones were extracted from Esri's 2022 land use data (Environmental Systems Research Institute, 2023).

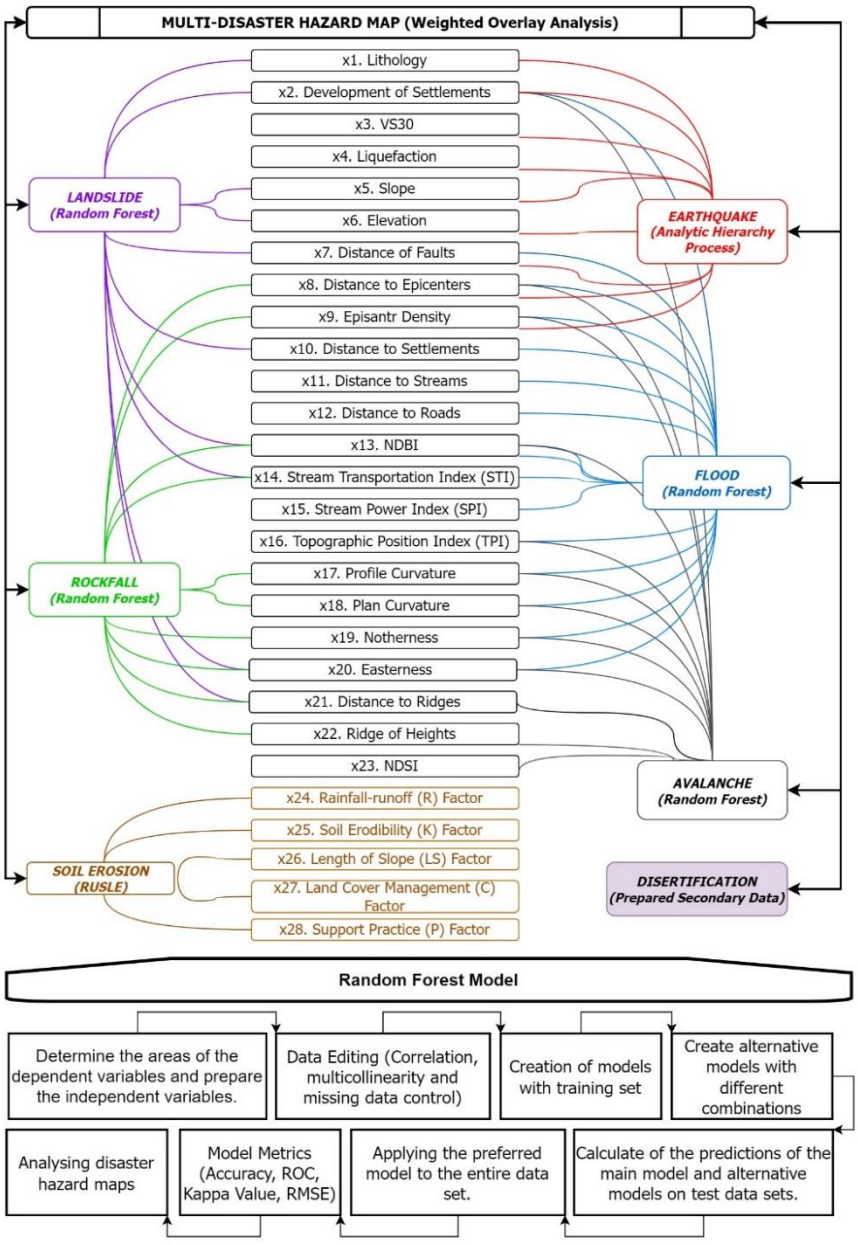

Figure 3. Methodology of this study

In order to make a hazard assessment of the major disasters in the province, the locations of the disaster sites were determined by confirming and redrawing the data obtained from AFAD, the Ministry of Agriculture and Forestry and the Elazığ Municipality with satellite imagery. Then, based on the literature, the spatial data required for each disaster were collected as much as possible and their correlations with the disasters were analysed. The models were simplified by performing multicollinearity analysis to avoid using unnecessary independent variables. Different machine learning models were used, among which the random forest algorithm was preferred, as it produces results more suitable for field observations. The maps produced were first analysed separately and then integrated with spatial overlap, and the results were interpreted through a multi-hazard map. The maps were created using ArcGIS, MATLAB, SAGA GIS, Python, and EARTH ENGINE tools (Figure 3).

Among the study's limitations, the most significant lies in the disparity of resolution within the obtained spatial data. Some data, like VS30, soil liquefaction, and soil classifications, maintain a resolution of approximately 250 meters, necessitating additional processing before their integration into the models. Despite precise interpolation, potential data gaps have impacted the quality of the models. The downscaling of land use data from 10 to 30 meters resolution was unproblematic. Alongside resolution challenges, the extensive and highly heterogeneous nature of the study area has constrained the analysis of resultant hazard maps. Finally, the simultaneous evaluation of numerous diverse hazard types has restricted the comprehensive analysis of previous studies pertaining to each individual hazard.

3.2. Analytic Hierarchy Process

The Analytic Hierarchy Process (AHP) is a decision-making model that helps us make decisions in our complex world. It's a three-part process that involves defining and organizing criteria, constraints and alternatives within a hierarchy to achieve decision objectives. The process involves evaluating pairwise comparisons between elements and synthesizing the results of pairwise comparisons at all levels using a solution algorithm (Saaty, 1980).

In the Analytic Hierarchy Process, the first stage requires each independent variable to be ranked according to its importance within its own category. This process establishes priorities among the variables within their own classes. A main pairwise comparison matrix is then constructed to determine the importance and order of priority of the independent variables in relation to each other. In this way, coefficients are obtained which indicate the priorities of the variables in relation to each other. The application of this method in practice requires careful consideration by the researcher or expert, both in classifying the variables and in determining their priorities in relation to each other. Finally, consistency ratios must be calculated, both between classes of variables and within the main comparison matrix (Özdağoğlu & Özdağoğlu, 2007).

To assess earthquake sensitivity, nine parameters were identified based on literature, expert opinions, field observations and local government databases (Pektezel, 2015; Jena et al., 2020; Yariyan et al., 2020; Özkazanç et al., 2020; Elazığ Provincial Directorate of Disaster and Emergency, 2021). The current situation of the area was initially presented within the framework of these parameters. Subsequently, a sensitivity analysis was conducted in alignment with expert-determined weights. The significance of these parameters, in terms of sensitivity, is as follows: Lithology, Development of Settlements, VS30, Distance to Liquefaction, Slope, Elevation, Fault Distance, Distance to Epicenters, and Epicenter Density. The variables were classified and paired with each other, resulting in the creation of five categories, ranging from very low to very high, each assigned the same weighting coefficients. The weighting consistency rate was obtained to be 2%. (Table 1).

Table 1. Pairwise comparison matrix for categories of variables

Lithology	Development of the Settlements	VS30	Distance to Liquefaction (m)	Slope (%)	Elevation	Fault Distance (m)	Distance to Epicenters (m)	Epicenter Density	*AHP*
Gneiss, schist, marble, etc. (Precambrian, Paleozoic)	Non-Settlement	650-952	0-100	40-217	1500-2603	31703-42549	14962-25102	0.0008-0.007	**0.062**
Unseparated ophiolite, diorite, gabbro, etc. (Mesozoic)	2011-2022	600-700	100-500	30-40	1250-1500	22526-31703	10139-14962	0.007-0.01	**0.099**
Basalt, granite, granodiorite, etc. (Cretaceous, Eocene, Lower Miocene)	2005-2010	500-600	500-1000	20-30	1150-1250	13181-22526	6595-10139	0.01-0.03	**0.161**
Unsorted clastics and carbonates, etc. (Upper Cretaceous, Upper Miocene, Pliocene)	2001-2005	400-500	1000-2000	10-20	1050-1150	5506-13181	3445-6595	0.03-0.05	**0.262**
Alluvial fans, unsorted Quaternary (Quaternary)	1985-2000	165-400	2000-17.300	0.01-10	665-1050	0.01-5506	0-3445	0.05-0.07	**0.416**
Consistency Ratio: %2									

In the second stage of binary comparison, following lithology, variables with higher earthquake impact levels, such as settlement development and VS30, were prioritized to indicate the degree of importance relative to each other.

In the pairwise comparison, which reflects the relative importance of the variables, weighting coefficients were determined with a 2% consistency ratio, ranging from 0.023 to 0.267. First, coefficients were assigned to variable classes by reclassification. Then, the weighting coefficients were assigned to the variables and the result map was obtained by calculating the sums (Table 2).

Table 2. Pairwise Comparison Matrix

Variables	Lithology	Development of the Settlements	VS30	Distance to Liquefaction (m)	Slope %	Elevation	Distance to Epicenters (m)	Fault Distance (m)	Epicenter Density	*AHP*
Lithology	1	1	2	3	4	5	6	7	8	***0.267***
Development of the Settlements		1	1	2	3	4	5	6	7	***0.211***
VS30			1	1	2	3	4	5	6	***0.159***
Distance to Liquefaction (m)				1	1	2	3	4	5	***0.115***
Slope %					1	1	2	3	4	***0.083***
Elevation						1	2	2	3	***0.064***
Fault Distance (m)							1	2	3	***0.046***
Distance to Epicenters (m)								1	2	***0.032***
Epicenter Density									1	***0.023***
Consistency Ratio: %2										

3.3. Random Forest Model

Random forests are an effective tool in prediction. The tool are a combination of tree predictors such that each tree depends on the values of a random vector sampled independently and with the same distribution for all trees in the forest (Breiman, 2001). The random forest algorithm is highly useful due to its ability to easily combine numerical, categorical, and mixed variables as predictors, operate efficiently in high-dimensional datasets, and adapt to non-linear relationships (Caiola & Reiter, 2010).

Different machine learning models have been used to identify disaster-affected areas, but among them, the Random Forest model, which has a more satisfactory spatial counterpart, has been preferred for the production of all disaster hazard maps. Indeed, this model has been used to produce disaster hazard maps for floods and inundations (Zhu & Zhang, 2022), landslides (Taalab et al., 2018), rockfalls (Hibert et al., 2017) and avalanches (Sielenou et al., 2021).

In the Random Forest algorithm, a large number of decision tree classifiers are first created, and then these classifiers are used to vote for test samples. The final decision is made by majority rule. Model selection in Random Forest involves selecting an appropriate number of classifiers from the many decision tree classifiers created, and then using these classifiers to vote for test samples (Zhu & Zhang, 2022). In Matlab, the equation used to implement the Random Forest model is as follows:

$$Mdl = TreeBagger(numTrees, X, y, 'Method', 'classification', 'OOBPrediction', 'on', 'NumPredictorsToSample', 'all'); \quad (1)$$

In the Random Forest algorithm, the number of trees and nodes is typically selected through trial and error, tailored to the specific problem (Sevgen & Tanrıvermiş, 2020). In this study, either 80% or 90% of the data was utilized as training data, with the remaining 10% or 20% allocated for testing. Sample sizes were adjusted based on the area of the dependent variables, with an attempt to maintain a roughly equal number of dependent and independent variables. A total of 15 trees were used in all models (represented by the 'numTrees' variable). The rest of the equation parameters indicate the use of a classification algorithm, which allows the calculation of the out-of-bag (OOB) error, and the use of all features at each tree node.

4. Results

In producing the disaster hazard maps, variable selection began with Spearman correlation analysis. Irrelevant factors were removed and the process repeated. Collinearity values were then calculated. It is important that there are no factors among the variables that perform the same function. The index used to check this is called the Variance Inflation Factor (VIF), which is expected to have a maximum value of 10 (Hair et al., 2014). Variables with collinearity values greater than 10 were further eliminated, completing the variable selection process.

Among the variables used in the earthquake hazard map, VS30, liquefaction and slope have a high correlation with each other and with other variables, while a similar aggregation is observed between elevation and epicentre variables. The correlation of other variables with each other is low (Figure 4).

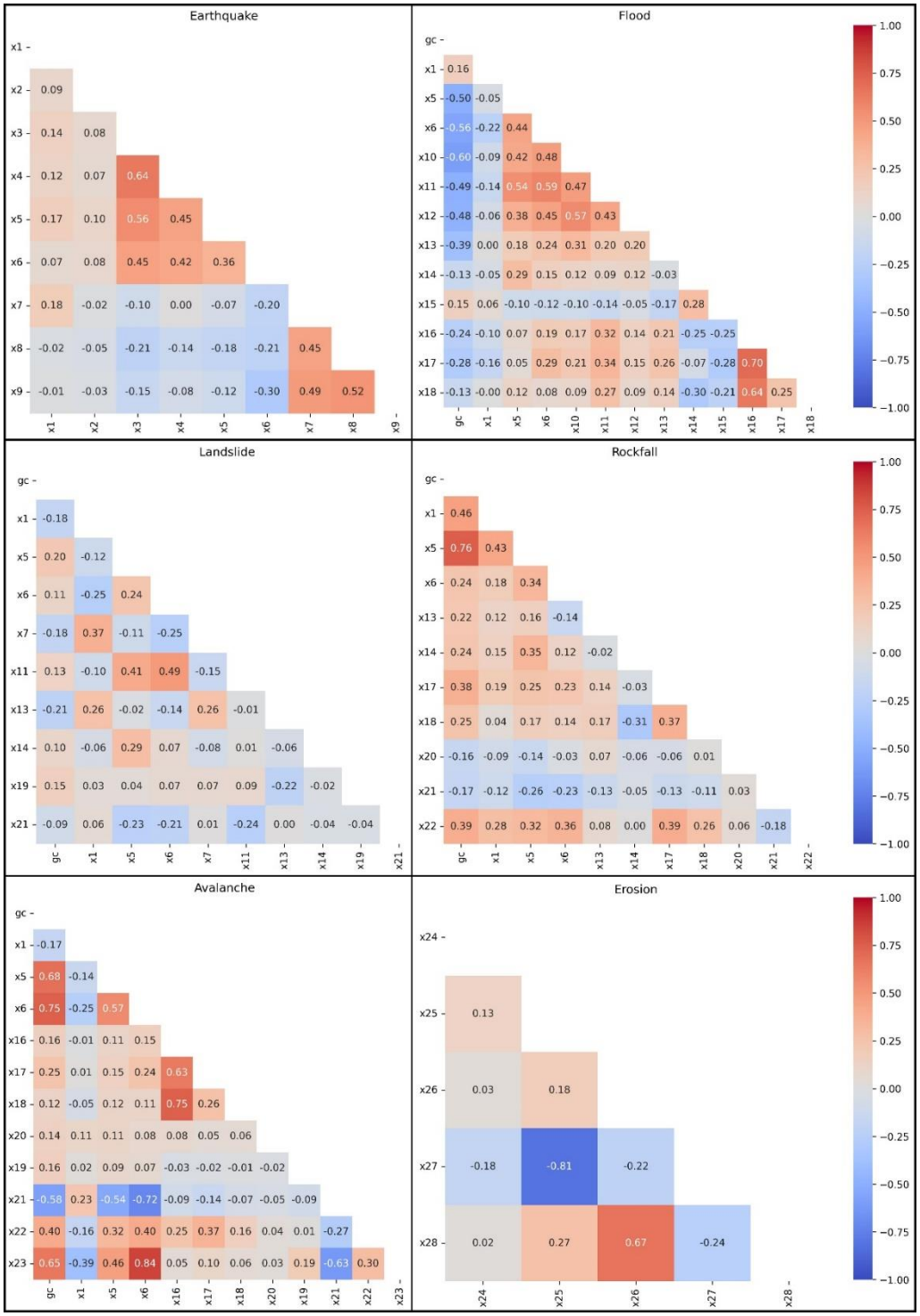

Figure 4: Correlation coefficients between dependent and independent variables according to disasters

For floods and inundations events, all variables except SPI generally show a negative and typically moderate relationship. Weak correlations are observed with distance to lakes, northerliness and easterliness. As with other disasters, the lithology data were transformed into continuous data using the frequency density method.

Landslide events show a moderate positive correlation with lithology and a moderate negative correlation with NDBI, while showing weak negative correlations with other variables.

For rockfall events, there is a moderate negative correlation with easterliness and distance to ridges. On the positive side, there is a strong correlation with slope and a moderate correlation with ridge height.

Avalanche formation is influenced by topographical features, weather conditions, the structure of the snowpack and natural and artificial triggers (Varol, 2022). With the exception of NDBI, all variables show a positive correlation with avalanche formation, and among these, elevation, slope and NDSI show the highest correlations in order.

The erosion susceptibility map was obtained using the RUSLE method. As erosion does not have a dependent variable, in terms of correlation between the effective factors, there is a moderate positive correlation between the LS factor and the P factor, while the correlation with the R factor is very low. There is a moderate negative correlation between the C factor and the K factor (Figure 4). As the desertification hazard map was obtained as a finished dataset, it was not subjected to correlation analysis.

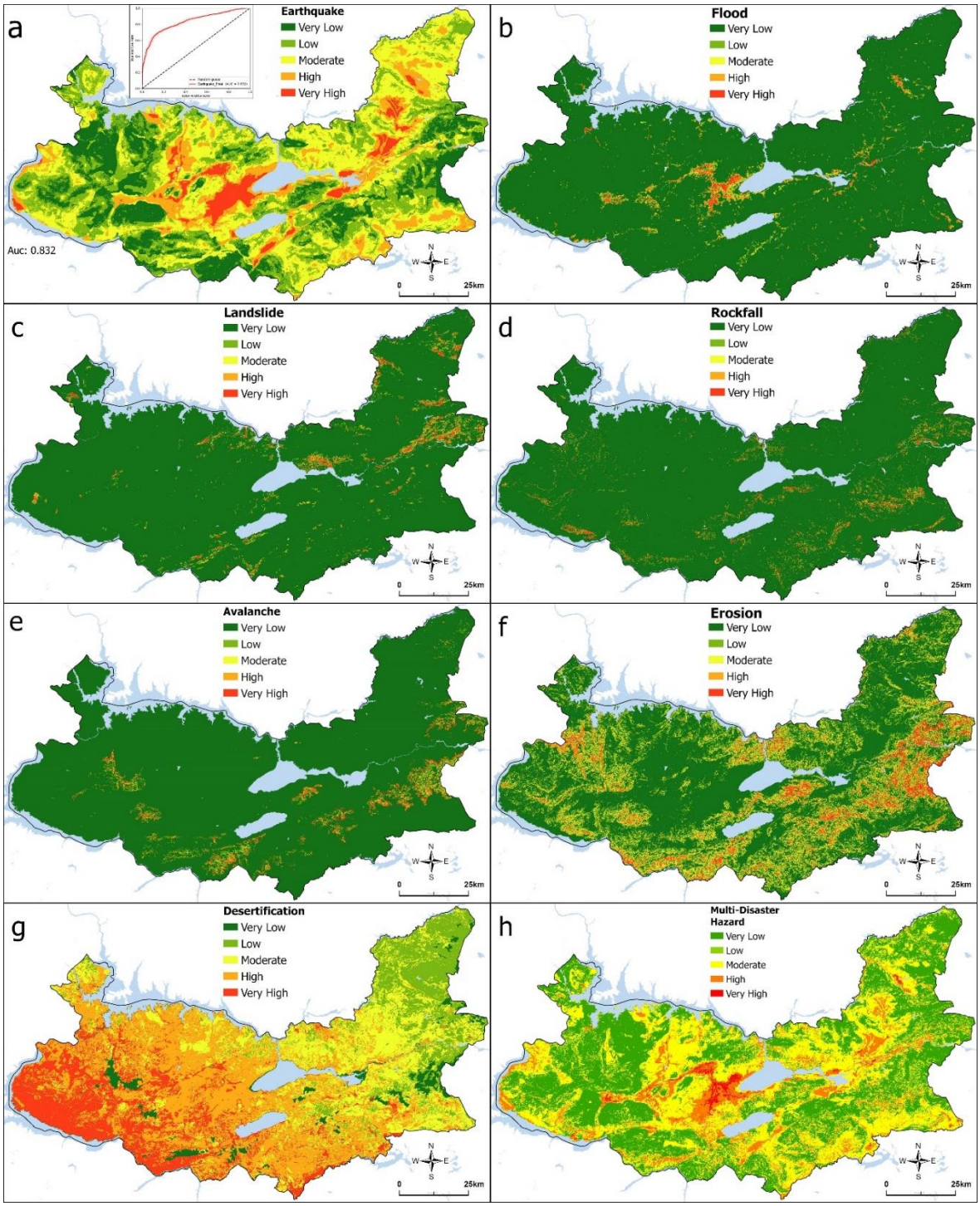

Figure 5: Disaster hazard maps and multi-disaster hazard map of Elazig Province

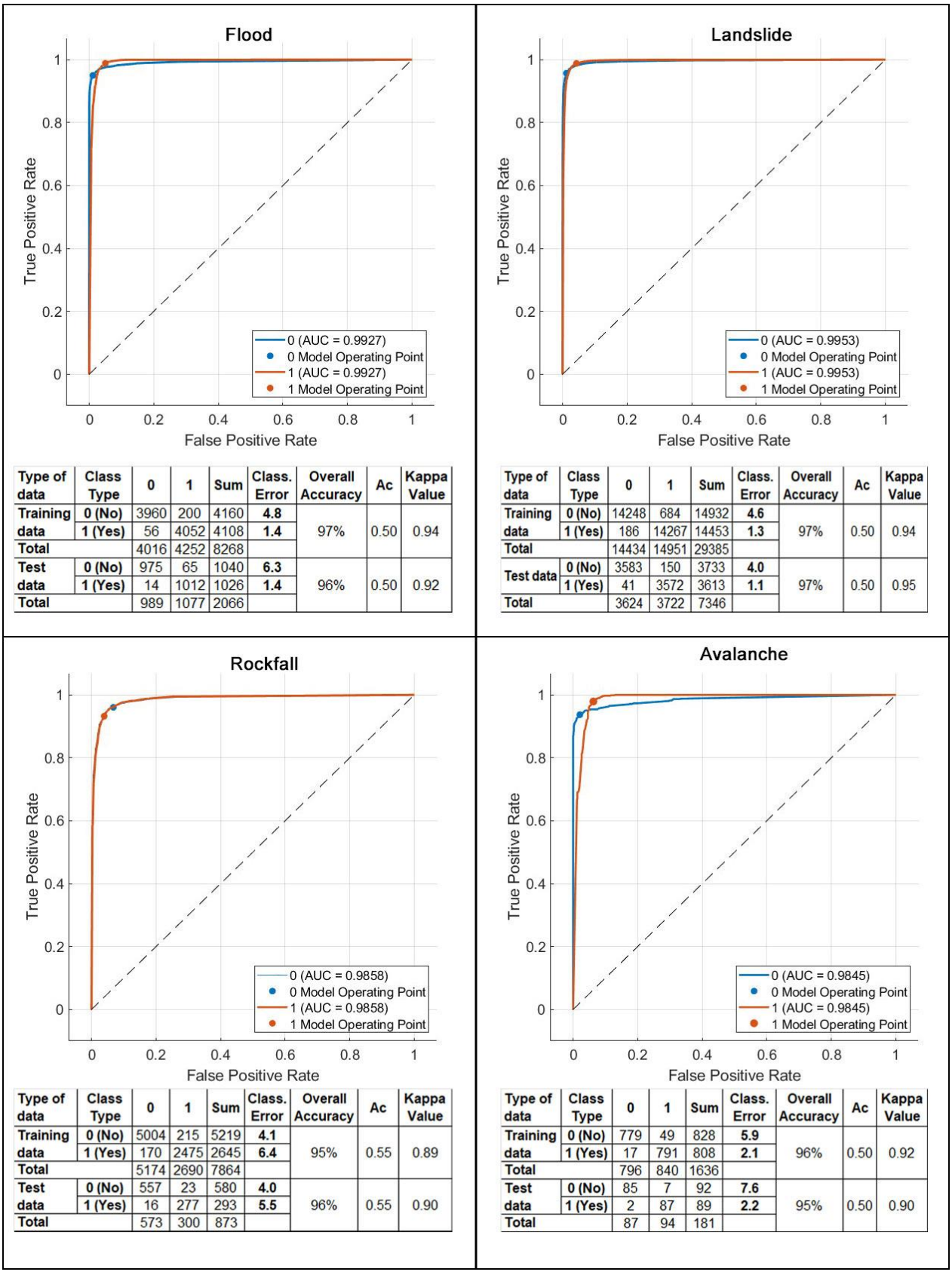

Type of data	Class Type	0	1	Sum	Class. Error	Overall Accuracy	Ac	Kappa Value
Training data	0 (No)	3960	200	4160	4.8	97%	0.50	0.94
	1 (Yes)	56	4052	4108	1.4			
Total		4016	4252	8268				
Test data	0 (No)	975	65	1040	6.3	96%	0.50	0.92
	1 (Yes)	14	1012	1026	1.4			
Total		989	1077	2066				

Type of data	Class Type	0	1	Sum	Class. Error	Overall Accuracy	Ac	Kappa Value
Training data	0 (No)	14248	684	14932	4.6	97%	0.50	0.94
	1 (Yes)	186	14267	14453	1.3			
Total		14434	14951	29385				
Test data	0 (No)	3583	150	3733	4.0	97%	0.50	0.95
	1 (Yes)	41	3572	3613	1.1			
Total		3624	3722	7346				

Type of data	Class Type	0	1	Sum	Class. Error	Overall Accuracy	Ac	Kappa Value
Training data	0 (No)	5004	215	5219	4.1	95%	0.55	0.89
	1 (Yes)	170	2475	2645	6.4			
Total		5174	2690	7864				
Test data	0 (No)	557	23	580	4.0	96%	0.55	0.90
	1 (Yes)	16	277	293	5.5			
Total		573	300	873				

Type of data	Class Type	0	1	Sum	Class. Error	Overall Accuracy	Ac	Kappa Value
Training data	0 (No)	779	49	828	5.9	96%	0.50	0.92
	1 (Yes)	17	791	808	2.1			
Total		796	840	1636				
Test data	0 (No)	85	7	92	7.6	95%	0.50	0.90
	1 (Yes)	2	87	89	2.2			
Total		87	94	181				

Figure 6. Validation metrics for random forest models of flood, landslide, rockfall and avalanche hazard maps

*Table 3: Distribution of buildings and agricultural land at risk according to disaster hazard result maps (km²)**

Class	Earthquake		Flood			Landslide		
	Area (km²)	Percentage of Buildings	Area (km²)	Agriculture Area (km²)	Percentage of Buildings	Area (km²)	Agriculture Area (km²)	Percentage of Buildings
Very Low	1598	3	8587	301	50.9	8925	457	88.5
Low	2622	10	144	40	10.6	155	3	1.4
Moderate	3256	24	432	69	15.6	60	2	4.3
High	1469	32	49	21	7.7	90	5	3.7
Very High	382	30	115	45	15.3	98	9	2.0
Total	9328	100.0	9328	476	100.0	9328	476	100.0

Class	Rockfall		Avalanche		Desertification		Erosion	
	Area (km²)	Percentage of Buildings (100 m. Buffer)	Area (km²)	Percentage of Buildings (100 m. Buffer)	Area (km²)	Agriculture Area (km²)	Area (km²)	Agriculture Area (km²)
Insignificant	8980	92.3	8910	98.0	881	9	6046	449
Weak	116	3.3	159	0.8	1228	14	1109	14
Considerable	56	1.8	79	0.6	2218	108	1244	10
Severe	78	1.6	34	0.4	3346	257	534	1
Very Severe	98	1.0	146	0.2	1654	89	395	2
Total	9328	100.0	9328	100.0	9328	476	9328	476

* *The table was produced by the author using reclassification and intersection analysis of the hazard maps produced as part of the research.*

4.1. Earthquake Hazard Assessment

In the province, the most seismically vulnerable areas are mainly in the southern and central parts of the plain, where the city of Elazığ is located (Tonbul et al., 2005; Palutoğlu & Tanyolu, 2006; Sunkar, 2014; Sertel, 2017).This area, which has the highest number of damaged buildings in the 2020 and 2023 earthquakes, is one of the priority zones that require sensitivity in the reconstruction process. Other high-risk areas in the province are the plains and lowlands corresponding to the East Anatolian Fault (EAF) and its extensions. These include the Uluova, Kovancılar, Hankendi, Sivrice and Çitli plains (Figure 5a).

High hazard areas extend from very hazardous areas to places where elevation and distance from faults increase. These areas include both plains and rugged terrain due to their proximity to fault lines. Partially hazardous areas are generally located on the lower slopes of mountainous areas. Low and very low hazard areas consist of rugged terrain corresponding to solid lithological units. However, buildings in these areas suffered significant damage in the 2020 earthquake. This is closely related to the age and structural characteristics of buildings and the duration of the earthquake.

For the accuracy analysis of the earthquake hazard map, the distribution of buildings requiring urgent demolition and those with severe damage in the 2020 earthquake was used, and this dataset consists of 1,000 building locations obtained through random sampling of buildings identified by AFAD as being at risk of collapse, severe or moderate damage following the 2020 Elazığ earthquake. Although predicting and assessing earthquake hazards is much more complex than predicting and assessing other disasters, the accuracy of the map is around 83% (Figure 5a).

62% of the province's buildings are located in very high and high hazard areas (Table 3). Most of the buildings situated in the areas classified as very high and high-risk are concentrated in densely urbanized regions, primarily in the provincial center. It is therefore essential to prepare the existing buildings against the hazard and to pay attention to the quality of the buildings to be constructed in these areas.

4.2. Floods and Inundations

Floods and inundations occur in the province due to snowmelt in the spring months and extreme rainfall events that exceed seasonal norms. For this reason, flood and inundation studies were carried out in various parts of the study area, particularly in the centre of the province (Sunkar & Bağcı, 2014; Korkmaz, 2022). In the study area, a positive trend of change in hourly extreme rainfall has been observed, especially in coastal areas (40-60%) (Albayrak, 2021; Dönmez, 2023). According to the Elazığ Province Disaster Risk Reduction Plan, there were no fatalities from flood disasters, but 9 disasters that caused property damage (Elazığ Provincial Directorate of Disaster and Emergency, 2021). Therefore, potential flood and flash flood events in the province should be taken as seriously as earthquakes, and preparedness and planning should be undertaken.

In producing the floods and inundations hazard map, the dependent variable was obtained by merging data from two different sources. The first source is the 100-year flood hazard areas found in the National Water Information System. Then, data from disasters that have occurred throughout the province since 1965, as documented by AFAD, were delineated on satellite imagery and merged. A significant proportion of these flood-prone areas have been relatively well prepared for disasters through the construction of drainage canals. However, there are still problems both with the capacity of these canals and with areas without flood control measures.

The central and southern parts of the Elazığ Plain, where settlement is most dense, are among the most vulnerable areas in the study area. The Şorşor Stream, which drains the Elazığ Plain, and the Kuyulu Stream, which drains the western part of Uluova, run along the Diyarbakır Highway, the Elazığ Airport, and the central part of the plain, which is affected by seasonal rivers in the northeast, putting a significant part of the towns of Yurtbaşı and Yazıkonak at risk (Figure 5b).

Other very high-risk areas in the province include Baskil town centre, Pınarlı village below Baskil, the section of the Keban Dam after the dam and downstream of the Keban stream, Maden town centre, Palu town centre, Beyhan town in Palu, the western part of Karakoçan town centre and several villages in the valleys and plains formed by the relatively large seasonal and perennial rivers. Secondary hazard areas are located around the very high hazard areas. Drainage channels have been constructed in certain sections of the existing very high-risk areas to reduce the impact of the hazard.

Areas at high and very high risk of floods and inundations account for about 2% of the province's total agricultural area and about 23% of the existing building stock (Table 3, Figure 5b).

The flood hazard map for the province was created using the Random Forest algorithm. The model validation metrics of the landslide hazard map were calculated as 99% in terms of AUC (area under curve), approximately 96% in terms of overall accuracy rate for training and test data, and 0.92 in terms of kappa value. The RMSE (root mean square error) value of the model was determined as 0.07 (Figure 6).

4.3. Landslide Hazard Assessment

The landslide map produced by the General Directorate of Mineral Research and Exploration was used to obtain the dependent variable for the landslide hazard map (General Directorate of Mineral Research and Exploration, 2023). However, to confirm these areas, polygons covering the crown and body of the landslide were manually drawn on recent satellite images.

According to the Disaster Risk Reduction Plan of Elazığ Province, 90 different mass movements (landslides, rockfalls and avalanches) have been reported in 76 settlements (Elazığ Provincial Directorate of Disaster and Emergency, 2021). In the province, the areas most prone to landslides are associated with factors such as slope angle, erosion and transport activities along the DAF and its extensions, as well as road construction and other human activities (Avci & Sunkar, 2018; Şengün et al., 2019). In terms of the number and size of these areas, Palu district is the most affected. In Palu, the presence of easily mobilized geological formations such as marl and limestone, combined with the potential for mass movements along the East Anatolian Fault line, has increased the potential for mass movements (Figure 5c).

The buildings located within 100 meters of very high and high landslide hazard areas represent approximately 6% of the total buildings in the province. In the agricultural area, 14 km2, or 0.15% of the total agricultural area, is located directly in the high landslide hazard area without buffer analysis (Table 3, Figure 5c).

The landslide hazard map for the province was created using the Random Forest algorithm. The model validation metrics of the landslide hazard map were calculated as 99% in terms of AUC (area under curve), approximately 97% in terms of overall accuracy rate for training and test data, and 0.95 in terms of kappa value. The RMSE (root mean square error) value of the model was determined as 0.07 (Figure 6).

4.4. Rockfall Hazard Assessment

In the case of rockfall hazards, the very high-risk areas are predominantly located in rugged terrain with high slopes and eroded slopes associated with specific lithological units throughout the province. Therefore, the probability of affecting populated areas is relatively low. The increase in hazard is associated with areas close to established settlements.

In order to obtain the rockfall hazard map, the existing erosion areas of the entire province and the locations indicated on the map of previous disasters belonging to AFAD were used. These areas were confirmed using satellite images and exaggerated drawings were reduced to derive the data again.

All the areas of very high and high rockfall hazard in the study area are generally located in rural areas, often far from settlements. However, some exceptions include the town centre of Maden and some villages, the surroundings of the town of Alacakaya and the village of Kuşsarayı in Baskil. Among the areas of relatively low risk, the most important is the rocky area north of the Ulukent neighborhood, east of Elazığ town. Rockfall is a relatively slow-moving hazard and can sometimes be overlooked. However, rockfall simulations should be carried out in high-risk areas, and structures in high-risk areas should be relocated. Buildings within 100 meters of high and very high rockfall hazard areas represent approximately 2.6% of the total buildings in the province (Table 3, Figure 5d).

The rockfall hazard map for the province was created using the Random Forest algorithm. The model validation metrics of the landslide hazard map were calculated as 98% in terms of AUC (area under curve), approximately 95% in terms of overall accuracy rate for training and test data, and 0.90 in terms of kappa value. The RMSE (root mean square error) value of the model was determined as 0.09 (Figure 6).

4.5. Avalanche Hazard Assessment

In the context of avalanche events, factors such as terrain ruggedness, high average elevation, slope inclination, and aspect play crucial roles (Elmastaş & Özcanlı, 2011). Therefore, the emphasis in detecting avalanche hazards has been placed on morphological factors.

Elazığ Province has encountered 10 snow avalanche incidents, as recorded in the existing disaster inventory (Elazığ Provincial Directorate of Disaster and Emergency, 2021). Despite the relatively low frequency of these incidents, the likelihood of recurrence is high, particularly during years with heavy snowfall, especially in the high mountainous areas of the province.

There is an area of 160 km² along the southern part of the province that is characterized by a high avalanche hazard. However, almost all of these areas are far from populated areas. Buildings within 100 meters of high and very high avalanche hazard areas represent approximately 0.7% of the total buildings in the province. It is a priority to relocate these buildings away from these hazard areas (Table 3, Figure 5e).

The avalanche hazard map for the province was created using the Random Forest algorithm. The model validation metrics of the landslide hazard map were calculated as 98% in terms of AUC (area under curve), approximately 95% in terms of overall accuracy rate for training and test data, and 0.90 in terms of kappa value. The RMSE (root mean square error) value of the model was determined as 0.12 (Figure 6).

4.6. Desertification Hazard Assessment

Desertification is defined as the degradation of land in arid, semi-arid and dry sub-humid areas due to various factors, including climate variability and human activities. Land degradation is a combination of processes such as soil erosion, deterioration of the economic properties of soils and long-term loss of natural vegetation resulting from factors such as desertification (United Nations, 1999). Thus, desertification is not limited to reduced rainfall, but is a process that can occur as a result of human activities and land management practices.

Land degradation related to desertification has become an increasingly important issue in the study area, particularly in the western part of the province, such as the Baskil and Keban basins, and a significant part of the central district. This high risk is due to the fact that these areas contain important agricultural land. Similar conditions exist in the low-lying areas of the Sivrice and Maden districts. The risk of desertification decreases as elevation increases towards the east and average rainfall increases. About 4% of the province's agricultural land is located in areas at high and very high risk of desertification (Table 3, Figure 5f).

The urban centre of Elazığ has experienced rapid population growth, accelerated industrialization, and the widespread adoption of modern agricultural practices. All these developments have increased the demand for and consumption of both surface and groundwater. Elazığ is one of the Turkish provinces where the trend of drought is increasing. It is estimated that the study area has a drought-prone character and the existing rainfall levels are expected to decrease further. Especially in a city where one-third of the precipitation occurs in the winter season, the intensification of winter drought is a significant indicator of this situation (Çelik et al., 2018).

4.7. Erosion Hazard Assessment

The Universal Soil Loss Equation (USLE) was developed in the mid-1960s to understand soil erosion for agricultural practices. It was updated in the mid-1980s to incorporate a significant amount of data accumulated since its original development and to include land use practices beyond agriculture, such as soil loss from mined areas. The revised version was renamed the Revised Universal Soil Loss Equation (RUSLE) (Sivakumar & Ndiang'ui, 2007). The RUSLE equation is A = R * K * LS * C * P, where A is soil loss, R is rainfall runoff erosion, K is soil erodibility factor, LS is slope length, C is land management and P is protection factor (Renard, 1997).

Soil erosion may not directly cause loss of life or property, but it has indirect effects that reduce the potential of the natural environment and increase the impact of floods. In arid soils, high temperatures and low rainfall often lead to low organic matter production and rapid oxidation. Low organic matter content, poor aggregation and low aggregate stability result in a high potential for wind and water erosion (Sivakumar & Ndiang'ui, 2007). In a semi-arid region such as the study area, the high risk of desertification in the western part further increases the intensity of erosion.

Approximately 30% of the study area is threatened by erosion, and these areas account for about 3% (13 km^2) of the total agricultural area in the province. Erosion-prone areas typically consist of high slopes and rugged terrain. In addition, the impact and intensity of other erosion-related disasters vary. In fact, in the province, areas with low vegetation cover, mainly around hilly areas such as Hasan Mountain, Hasret Mountain, Asker Mountain and similar terrains, are more affected by floods and flash floods due to heavy rainfall (Table 3, Figure 5g).

4.8. Multi-Disaster Hazard Assessment

There are several approaches to producing multihazard hazard maps. One of these approaches is synthesis maps, which are obtained by combining maps. In these maps, each pixel is evaluated by dividing it into separate categories according to the disaster types to which it belongs (Pourghasemi et al., 2019). The second approach is the Mamdani Fuzzy Inference System", which reduces uncertainty using if-then rules. When combining maps in the system, blurring, rule evaluation, aggregation and defuzzification are performed (Yanar et al., 2020). Another approach is the "Weighted Linear Combination" method, which is also used in this study. The combination is made using the weights assigned to the hazard outcome maps. (Rehman et al., 2022).

$$MSI = \sum_{i=1}^{n} H_i \times W_i \quad (2)$$

To produce the multiple disaster hazard map, all the individual hazard maps were merged using the weighted overlay tool. Each hazard was weighted as follows: earthquake 25%, flood 25%, landslide 10%, rockfall 10%, avalanche 10%, erosion 10% and desertification 10%. The weighting values were determined on the basis of field observations. As a result, very high hazard areas, in terms of multiple disasters, cover an area of 11 km^2 and high hazard areas cover an area of 152 km^2. A total area of 163 km^2 contains about half of the existing buildings and about 10% of the agricultural land (Figure 5h).

The process of producing the multiple disaster hazard map involves several challenges, such as selecting which disasters to include, determining which variables to use, identifying and delineating disaster-prone areas, selecting algorithms, and combining these individual maps. Therefore, while there may be commonalities in disaster-related studies, there can be significant differences in methodology and approach. As a natural consequence of the problems associated with disasters, the future of this process will undoubtedly change according to needs. However, the multidimensional nature of disasters makes it essential to address them in a comprehensive and interdisciplinary manner.

Integrated disaster risk analyses are therefore a healthier approach to solving spatial problems. They should take into account that disasters are a multidisciplinary phenomenon. The use of artificial intelligence-based systems for real-time data monitoring and instant situation analysis has become an inevitable requirement for disaster management and resilience.

5. Conclusion

Elazig is a province in Türkiye that has been affected by numerous disasters, mainly earthquakes, floods, and flash floods. In this context, hazard maps for earthquakes, floods, flash floods, landslides, rockfalls, avalanches, desertification, and erosion were prepared to analyze disaster risks. These maps were then combined to produce a multi-hazard map. The Analytical Hierarchy Process (AHP) was used for the earthquake hazard map, the Revised Universal Soil Loss Equation (RUSLE) for the erosion hazard map, and the Random Forest algorithm, a machine learning model, for the flood, landslide, rockfall, and avalanche hazards.

This study aims to enhance Elazig's disaster preparedness, improve resource allocation, and speed up the post-disaster recovery process by creating a spatial synthesis and database. A total of 30 different independent variables were analyzed for correlation and multicollinearity, and the relevant variables were selected for each type of disaster. The resulting hazard maps were subjected to an accuracy assessment using a 10-20% slice of the dataset, resulting in prediction rates of 90% and above.

Throughout the province, the average building size is approximately 180 m². The area around the building varies from 500 m² to 1000 m². Since each pixel in the generated hazard maps corresponds to an area of approximately 961 m², this data source can be used as a functional resource for selecting locations for new residential buildings.

In conclusion, the comprehensive hazard assessment conducted in Elazig Province reveals multifaceted risks across seismic, hydrological, geological, and environmental domains. Earthquake-prone areas, especially in the southern and central plains, stand as critical zones, particularly evident from the substantial damages incurred in recent earthquakes. Floods and inundations pose significant threats, accentuated by observed trends of extreme rainfall events, urging a serious preparedness approach. Landslide hazards, influenced by factors like slope angles and human activities, affect various areas, notably the Palu district.

Rockfall hazards primarily pose risks in rural, rugged terrains, occasionally impacting populated regions. Avalanche incidents, while infrequent, carry recurring possibilities, predominantly in high mountainous zones, warranting strategic dwelling relocations. Desertification and erosion risks, tied to land degradation and climatic variations, showcase vulnerabilities, notably in the western parts, affecting agricultural productivity.

Combining single-hazard maps into a comprehensive multi-hazard assessment has identified extensive high-risk areas, including substantial proportions of buildings and agricultural land. However, this integration process presented challenges in methodology and variable selection, highlighting the need for a unified approach in disaster risk analysis.

Moving forward, a multidimensional understanding and response to these risks are imperative. Addressing disasters necessitates an interdisciplinary approach, which emphasizes real-time data monitoring and advanced analytical systems for effective disaster management and resilience.

The findings underline the importance of proactive planning, preparedness, and mitigation strategies to safeguard lives, properties, and the environment in Elazig Province against the diverse array of hazards. Furthermore, disaster-related hazard analysis should be used not only to improve the current situation but also to inform land use decisions. This multi-hazard map is valuable for both government agencies and individuals. While government agencies have access to such maps, individual consumers may find it difficult to obtain this information. Web-based applications are therefore essential for increasing public awareness of hazardous areas, which is vital for the safety of life and property.

References

Abdulkadhim, A. H. (2019). Estimating snow cover area in south of Turkey using the Normalized Difference Snow Index (NDSI) form MODIS Satellite Images. *Journal of Physics: Conference Series*, *1279*(1), Article 12047. https://doi.org/10.1088/1742-6596/1279/1/012047.

Aksha, S. K., Resler, L. M., Juran, L., & Carstensen, L. W. (2020). A geospatial analysis of multi-hazard risk in Dharan, Nepal. *Geomatics, Natural Hazards and Risk*, *11*(1), 88–111. https://doi.org/10.1080/19475705.2019.1710580

Albayrak, D. (2021). *The impact of climate change on future extreme precipitation in Turkey* [Master's thesis, Istanbul Technical University]. CoHE Thesis Center. https://tez.yok.gov.tr/UlusalTezMerkezi

Avci, V., & Sunkar, M. (2018). The relationship of landslides with lithological units and fault lines occurring on the East Anatolian Fault Zone, between Palu (Elazığ) and Bingöl, Turkey. *Bulletin of the Mineral Research and Exploration*, 157, 23–38. https://doi.org/10.19111/bulletinofmre.428277

Bilgiç, T. (2002). *1: 500 000 scale Turkey Geological Map Series, Sivas sheet*. Maden Tetkik ve Arama Genel Müdürlüğü, Ankara. Retrieved June 9, 2023, https://www.mta.gov.tr/v3.0/hizmetler/500bas

Boğaziçi Üniversitesi Kandilli Rasathanesi ve Deprem Araştırma Enstitüsü. (2023). *Regional Earthquake-Tsunami Monitoring and Evaluation Center - Earthquake Catalog*. Retrieved June 6, 2023, http://www.koeri.boun.edu.tr/sismo/zeqdb/

Breiman, L. (2001). Random forests. *Machine Learning*, *45*(1), 5–32. https://doi.org/10.1023/A:1010933404324

Brown, C. F., Brumby, S. P., Guzder-Williams, B., Birch, T., Hyde, S. B., Mazzariello, J., et al. (2022). Dynamic World, near real-time global 10 m land use land cover mapping. *Scientific Data*, *9*(1), 1–17. https://doi.org/10.1038/s41597-022-01307-4

Caiola, G., & Reiter, J. P. (2010). Random forests for generating partially synthetic, categorical data. *Transactions on Data Privacy*, *3*(1), 27–42.

Corominas, J., Copons, R., Vilaplana, J. M., Altimir, J., & Amigó, J. (2003). Integrated landslide susceptibility analysis and hazard assessment in the Principality of Andorra. *Natural Hazards*, *30*(3), 421–435.

Çelik, M. A., Kopar, İ., & Bayram, H. (2018). Doğu Anadolu Bölgesi'nin Mevsimlik Kuraklık Analizi. *ATASOBED*, *22*(3), 1741–1761.

Das, S. (2019). Geospatial mapping of flood susceptibility and hydro-geomorphic response to the floods in Ulhas basin, India. *Remote Sensing Applications: Society and Environment*, *14*, 60–74. https://doi.org/10.1016/j.rsase.2019.02.006

Disaster and Emergency Management Presidency. (2023). *Earthquake Catalog*. Disaster and Emergency Management Presidency (AFAD). Retrieved June 6, 2023, https://deprem.afad.gov.tr/event-catalog

Dönmez, K. (2023). *Future changes in hourly extreme precipitation, return levels, and non-stationary impacts in Türkiye* [Master's thesis, Istanbul Technical University]. CoHE Thesis Center. https://tez.yok.gov.tr/UlusalTezMerkezi.

Duman, T., Emre, Ö., Özalp, S., Elmacı, H., & Olgun, Ş. (2012). *1:250000 scale Turkey Active Fault Map Series, NJ37-7*. Maden Tetkik ve Arama Genel Müdürlüğü, Ankara. Retrieved June 9, 2023, https://www.mta.gov.tr/v3.0/hizmetler/diri-fay-haritalari

Earth Resources Observation and Science Center. (2017). *Shuttle Radar Topography Mission (SRTM) 1 Arc-Second Global*. Retrieved June 6, 2023, https://earthexplorer.usgs.gov

Efiong, J., Eni, D. I., Obiefuna, J. N., & Etu, S. J. (2021). Geospatial modelling of landslide susceptibility in Cross River State of Nigeria. *Scientific African*, *14*, Article e01032. https://doi.org/10.1016/j.sciaf.2021.e01032

Ekmekcioğlu, Ö., Koc, K., & Özger, M. (2021). Stakeholder perceptions in flood risk assessment: A hybrid fuzzy AHP-TOPSIS approach for Istanbul, Turkey. *International Journal of Disaster Risk Reduction*, *60*, Article 102327. https://doi.org/10.1016/j.ijdrr.2021.102327

Elazığ Provincial Directorate of Disaster and Emergency. (2021). *Elazığ İl Afet Risk Azaltma Planı*. Retrieved February 2, 2023, https://elazig.afad.gov.tr/kurumlar/elazig.afad/E-Kutuphane/Il-Planlari/Elazig_irap__3103.pdf

Elmastaş, N., & Özcanlı, M. (2011, 3-5 Kasım). *Bitlis İlinde Çığ Afet Alanlarının Tespiti ve Çığ Risk Analizi* [Bildiri Sunumu]. VI. Ulusal Coğrafya Sempozyumu, Ankara, Türkiye.

Environmental Systems Research Institute. (2023). *Sentinel-2 10m Land Use/Land Cover Time Series*. ESRI. Retrieved June 6, 2023, https://www.arcgis.com/home/item.html ?id=d3da5dd386d140cf93fc9ecbf8da5e31

Gall, M., Nguyen, K. H., & Cutter, S. L. (2015). Integrated research on disaster risk: Is it really integrated? *International Journal of Disaster Risk Reduction*, *12*, 255–267. https://doi.org/10.1016/j.ijdrr.2015.01.010

General Directorate of Mineral Research and Exploration. (2023). *GeoScience Map Viewer*. General Directorate of Mineral Research and Exploration (MTA). Retrieved June 6, 2023, http://yerbilimleri.mta.gov.tr/

GEOFABRIK. (2023). *OpenStreetMap Data Extracts*. Retrieved June 6, 2023, https://download.geofabrik.de/europe/turkey.html

Gill, J. C., & Malamud, B. D. (2014). Reviewing and visualizing the interactions of natural hazards. *Reviews of Geophysics*, *52*(4), 680–722. https://doi.org/10.1002/2013RG000445

Hair, J. F., Black, W. C., Babin, B. J., & Anderson, R. E. (2014). *Multivariate data analysis. Pearson new international seventh edition*. Pearson.

Harff, J., Meschede, M., Petersen, S., & Thiede, J. (Eds.). (2016). *Encyclopedia of marine geosciences*. Springer Science+Business Media.

Heath, D. C., Wald, D. J., Worden, C. B., Thompson, E. M., & Smoczyk, G. M. (2020). A global hybrid V S30 map with a topographic slope-based default and regional map insets. *Earthquake Spectra*, *36*(3), 1570–1584. https://doi.org/10.1177/8755293020911137

Hibert, C., Provost, F., Malet, J. P., Maggi, A., Stumpf, A., & Ferrazzini, V. (2017). Automatic identification of rockfalls and volcano-tectonic earthquakes at the Piton de la Fournaise volcano using a Random Forest algorithm. *Journal of Volcanology and Geothermal Research*, *340*, 130–142. https://doi.org/10.1016/j.jvolgeores.2017.04.015

Hutter, B. M. (Ed.). (2017). *Risk, resilience, inequality and environmental law*. Edward Elgar Publishing.

Jena, R., Pradhan, B., Beydoun, G., Nizamuddin, Ardiansyah, Sofyan, H., & Affan, M. (2020). Integrated model for earthquake risk assessment using neural network and analytic hierarchy process: Aceh province, Indonesia. *Geoscience Frontiers*, *11*(2), 613–634. https://doi.org/10.1016/j.gsf.2019.07.006

Jha, A. K., Miner, T. W., & Stanton-Geddes, Z. (2013). *Building urban resilience: Principles, tools, and practice*. World Bank.

Kappes, M. S., Keiler, M., von Elverfeldt, K., & Glade, T. (2012). Challenges of analyzing multi-hazard risk: A review. *Natural Hazards*, *64*(2), 1925–1958. https://doi.org/10.1007/s11069-012-0294-2

Khosravi, K., Nohani, E., Maroufinia, E., & Pourghasemi, H. R. (2016). A GIS-based flood susceptibility assessment and its mapping in Iran: A comparison between frequency ratio and weights-of-evidence bivariate statistical models with multi-criteria decision-making technique. *Natural Hazards*, *83*(2), 947–987. https://doi.org/10.1007/s11069-016-2357-2

Knijff, J. M., Jones, R. J. A., & Montanarella, L. (2000). *Soil erosion risk assessment in Europe*. European Soil Bureau, European Commission.

Koks, E. E., Rozenberg, J., Zorn, C., Tariverdi, M., Vousdoukas, M., Fraser, S. A., et al. (2019). A global multi-hazard risk analysis of road and railway infrastructure assets. *Nature Communications*, *10*(1), Article 2677. https://doi.org/10.1038/s41467-019-10442-3

Korkmaz, M. (2022). Taşkın risk analizinde HEC-RAS modellemesinin kullanımı. *NWSA Engineering Sciences*, *17*(4), 54–66. https://doi.org/10.12739/NWSA.2022.17.4.1A0482

Korup, O., Clague, J. J., Hermanns, R. L., Hewitt, K., Strom, A. L., & Weidinger, J. T. (2007). Giant landslides, topography, and erosion. *Earth and Planetary Science Letters*, *261*(3-4), 578–589. https://doi.org/10.1016/j.epsl.2007.07.025

Li, Y., Osei, F. B., Hu, T., & Stein, A. (2023). Urban flood susceptibility mapping based on social media data in Chengdu city, China. *Sustainable Cities and Society*, *88*, Article 104307. https://doi.org/10.1016/j.scs.2022.104307

Marzocchi, W., Garcia-Aristizabal, A., Gasparini, P., Mastellone, M. L., & Di Ruocco, A. (2012). Basic principles of multi-risk assessment: A case study in Italy. *Natural Hazards*, *62*(2), 551–573. https://doi.org/10.1007/s11069-012-0092-x

Özdağoğlu, A., & Özdağoğlu, G. (2007). Comparison of AHP and fuzzy AHP for the multi-criteria decision making processes with linguistic evaluations. *İstanbul Ticaret Üniversitesi Fen Bilimleri Dergisi*, *6*(11), 65–85.

Özkazanç, S., Sıddıqui, D. S., & Güngör, M. (2020). Sensitivity analysis of earthquake using the Analytic Hierarchy Process (AHP) method: Sample of Adana. *İDEALKENT*, *11*(30), 570–591.

Palutoğlu, M., & Tanyolu, E. (2006). Elazığ İl Merkezi Yerleşim Alanının Depremselliği. *Fırat University, Journal of Science and Engineering*, *18*(4), 577-588.

Panagos, P., Borrelli, P., & Meusburger, K. (2015). A new European slope length and steepness factor (LS-Factor) for modeling soil erosion by water. *Geosciences*, *5*(2), 117–126. https://doi.org/10.3390/geosciences5020117

Panagos, P., Hengl, T., Wheeler, I., Marcinkowski, P., Rukeza, M. B., Yu, B., et al. (2023). Global rainfall erosivity database (GloREDa) and monthly R-factor data at 1 km spatial resolution. *Data in Brief*, *50*, Article 109482. https://doi.org/10.1016/j.dib.2023.109482

Pektezel, H. (2015). Coğrafi bilgi sistemleri (CBS) ve analitik hiyerarşi sistemine (AHS) göre Gelibolu Yarımadası'nın deprem duyarlılık analizi. *The Journal of Academic Social Science Studies*, *36*, 179–201.

Poggio, L., de Sousa, L. M., Batjes, N. H., Heuvelink, G., Kempen, B., Ribeiro, E., & Rossiter, D. (2021). SoilGrids 2.0: Producing soil information for the globe with quantified spatial uncertainty. *SOIL*, *7*, 217–240. https://doi.org/10.5194/soil-7-217-2021

Pourghasemi, H. R., Gayen, A., Panahi, M., Rezaie, F., & Blaschke, T. (2019). Multi-hazard probability assessment and mapping in Iran. *The Science of the Total Environment*, *692*, 556–571. https://doi.org/10.1016/j.scitotenv.2019.07.203

Rehman, A., Song, J., Haq, F., Mahmood, S., Ahamad, M. I., Basharat, M., et al. (2022). Multi-hazard susceptibility assessment using the Analytical Hierarchy Process and Frequency Ratio techniques in the Northwest Himalayas, Pakistan. *Remote Sensing*, *14*(3), Article 554. https://doi.org/10.3390/rs14030554

Renard, K. G. (1997). *Predicting soil erosion by water: A guide to conservation planning with the revised universal soil loss equation (RUSLE)*. U.S. Dept. of Agriculture, Agricultural Research Service.

Rodriguez, F., Maire, E., Courjault-Radé, P., & Darrozes, J. (2002). The Black Top Hat function applied to a DEM: A tool to estimate recent incision in a mountainous watershed (Estibère Watershed, Central Pyrenees). *Geophysical Research Letters*, *29*(6), Article 1085. https://doi.org/10.1029/2001GL014412

Rogelis, M. C. (2015). *Flood Risk in Road Networks*. Retrieved August 12, 2023, http://hdl.handle.net/10986/2298

Rusydi, H., Effendi, R., & Rahmawati, R. (2017). Vulnerability zoning of earthquake disaster of Palu. *International Journal of Science and Applied Science: Conference Series*, *1*(2), 137–143.

Saaty, T. L. (1980). *The analytic hierarchy process: Planning, priority setting, resource allocation*. McGraw-Hill International.

Sahana, M., & Patel, P. P. (2019). A comparison of frequency ratio and fuzzy logic models for flood susceptibility assessment of the lower Kosi River Basin in India. *Environmental Earth Sciences*, *78*(10), 1–27. https://doi.org/10.1007/s12665-019-8285-1

Schicker, R., & Moon, V. (2012). Comparison of bivariate and multivariate statistical approaches in landslide susceptibility mapping at a regional scale. *Geomorphology*, *161-162*, 40–57. https://doi.org/10.1016/j.geomorph.2012.03.036

Sertel, S. (2017). Elazığ'da meydana gelen afetler (1931-1980). *Akademik Sosyal Araştırmalar Dergisi*, *49*, 132-162.

Sevgen, C. S., & Tanrıvermiş, A. Y. (2020). Mass appraisal with a machine learning algorithm: Random forest regression. *Bilişim Teknolojileri Dergisi*, *13*(3), 301–311. https://doi.org/10.17671/gazibtd.555784

Shin, G. J. (1999). *The Analysis of Soil Erosion Analysis in Watershed Using GIS* [Ph.D. Dissertation, Gang-Won National University]. Retrieved August 12, 2023, https://www.scirp.org/reference/referencespapers?referenceid=674937

Sielenou, P. D., Viallon-Galinier, L., Hagenmuller, P., Naveau, P., Morin, S., Dumont, M., et al. (2021). Combining random forests and class-balancing to discriminate between three classes of avalanche activity in the French Alps. *Cold Regions Science and Technology, 187*, Article 103276. https://doi.org/10.1016/j.coldregions.2021.103276

Sivakumar, M. V. K., & Ndiang'ui, N. (2007). *Climate and land degradation*. Springer.

Sunkar, M. (2014). 8 Mart 2010 Kovancılar-Okçular (Elazığ) depremi; yapı malzemesi ve yapı tarzının can ve mal kayıpları üzerindeki etkisi. *Turkish Geography Review, 56*, 23–37. https://doi.org/10.17211/tcd.18070

Sunkar, M., & Bağcı, H. R. (Eds.). (2014). Uluova'nın kuzeydoğusunda (Elazığ) yaşanan sel ve taşkın olaylarının çevresel etkileri. In M. Ertürk, A. Uzun, & Ş. Danacıoğlu (Eds.), *Türkiye Coğrafyacılar Derneği Uluslararası Kongresi*. Türkiye Coğrafyacılar Derneği Uluslararası Kongresi, Muğla, Türkiye.

Sutley, E. J., van de Lindt, J. W., & Peek, L. (2017). Multihazard analysis: Integrated engineering and social science approach. *Journal of Structural Engineering, 143*(9), Article 04017107. https://doi.org/10.1061/(ASCE)ST.1943-541X.0001846

Şengün, M, T., Şaman, B., & Karadeniz, E. (2019). Kalaba Road (Sivrice-Elazığ) landslide and susceptibility analysis. In B. Gonencgil, T. A. Ertek, I. Akova & E. Elbasi (Eds.), *1st Istanbul International Geography Congress Proceedings Book* (pp. 642-652). Istanbul University Press.

Taalab, K., Cheng, T., & Zhang, Y. (2018). Mapping landslide susceptibility and types using Random Forest. *Big Earth Data, 2*(2), 159–178. https://doi.org/10.1080/20964471.2018.1472392

Tarhan, N. (2002). *1: 500 000 scale Turkey Geological Map Series, Erzurum sheet*. Maden Tetkik ve Arama Genel Müdürlüğü, Ankara. Retrieved June 9, 2023, https://www.mta.gov.tr/v3.0/hizmetler/500bas

Tehrany, M. S., Jones, S., & Shabani, F. (2019). Identifying the essential flood conditioning factors for flood prone area mapping using machine learning techniques. *Catena, 175*, 174–192. https://doi.org/10.1016/j.catena.2018.12.011

Tonbul, S., Karadogan, S., & Özcan, N. (2005, April, 27-29). *Elazığ kenti ve yakın çevresi için CBS ortamında olası doğal risk değerlendirmesi ve afet bilgi sistemi örnek uygulaması* [Bildiri Sunumum], Ege Coğrafi Bilgi Sistemleri Sempozyumu, İzmir, Türkiye.

Tonini, M., D'Andrea, M., Biondi, G., Degli Esposti, S., Trucchia, A., & Fiorucci, P. (2020). A machine learning-based approach for wildfire susceptibility mapping: The case study of the Liguria region in Italy. *Geosciences, 10*(3), Article 105. https://doi.org/10.3390/geosciences10030105

Toprak, A., & Canpolat, F. A. (2022). Frekans oran, analitik hiyerarşi ve lojistik regresyon modellerinin taşkın tehlike tahmininde karşılaştırmalı kullanımı, Fatsa ilçe merkezi ve yakın çevresi örneği. *International Journal of Geography and Geography Education, 45*, 349–379. https://doi.org/10.32003/igge.998492

Turkish Statistical Institute. (2023). *Demographic Statistics in Turkey*. Turkish Statistical Institute (TURKSTAT). Retrieved May 12, 2023 https://biruni.tuik.gov.tr/medas/?kn=95&locale=en

United Nations. (1999). *United Nations Convention to Combat Desertification. In those countries experiencing serious drought and/or desertification, particularly in Africa*. https://catalogue.unccd.int/936_UNCCD_Convention_ENG.pdf

United Nations Department of Public Information. (1994). *Agenda 21: Programme of action for sustainable development; Rio Declaration on Environment and Development; Statement of forest principles*. United Nations Environment Programme (UNEP). https://unesdoc.unesco.org/ark:/48223/pf0000116639

United Nations Office for Disaster Risk Reduction. (2022). *Global Assessment Report on Disaster Risk Reduction 2022: Our world at risk: Transforming governance for a resilient future*. United Nations Office for Disaster Risk Reduction (UNDRR). https://www.undrr.org/gar/gar2022-our-world-risk-gar

UNEP. (2004). *Guidelines for the application of environmental risk assessment in the European Union*. Earthprint.

Varol, N. (2022). Avalanche susceptibility mapping with the use of frequency ratio, fuzzy and classical analytical hierarchy process for Uzungol area, Turkey. *Cold Regions Science and Technology, 194*, Article 103439. https://doi.org/10.1016/j.coldregions.2021.103439

Weiss, A. (2001). *Topographic position and landforms analysis* [Conference presentation]. ESRI User Conference, San Diego, United States. Retrieved May 12, 2023, http://jennessent.com/downloads/TPI-poster-TNC_18x22.pdf

Wischmeier, W. H., & Smith, D. D. (1958). Rainfall energy and its relationship to soil loss. *Eos, Transactions American Geophysical Union, 39*(2), 285–291. https://doi.org/10.1029/TR039i002p00285

World Settlement Footprint. (2023). *World Settlement Footprint (WSF) Evolution - Landsat-5/-7 - Global*. Retrieved December 12, 2023, https://download.geoservice.dlr.de/WSF_EVO/#details

Yanar, T., Kocaman, S., & Gokceoglu, C. (2020). Use of Mamdani fuzzy algorithm for multi-hazard susceptibility assessment in a developing urban settlement (Mamak, Ankara, Turkey). *International Journal of Geo-Information, 9*(2), Article 114. https://doi.org/10.3390/ijgi9020114

Yanis, M., & Furumoto, Y. (2019). Lithological identification of devastated area by Pidie Jaya earthquake through Poisson's ratio analysis. *International Journal of GEOMATE, 17*(63), 210-216. https://doi.org/10.21660/2019.63.77489

Yariyan, P., Zabihi, H., Wolf, I. D., Karami, M., & Amiriyan, S. (2020). Earthquake risk assessment using an integrated Fuzzy Analytic Hierarchy Process with Artificial Neural Networks based on GIS: A case study of Sanandaj in Iran. *International Journal of Disaster Risk Reduction, 50*, Article 101705. https://doi.org/10.1016/j.ijdrr.2020.101705

Yeon, Y. K., Han, J. G., & Ryu, K. H. (2010). Landslide susceptibility mapping in Injae, Korea, using a decision tree. *Engineering Geology, 116*(3-4), 274–283. https://doi.org/10.1016/j.enggeo.2010.09.009

Zengin, B., & Aydin, F. (2023). The effect of material quality on buildings moderately and heavily damaged by the Kahramanmaraş earthquakes. *Applied Sciences, 13*(19), Article 10668. https://doi.org/10.3390/app131910668

Zhou, J., Huang, S., Wang, M., & Qiu, Y. (2022). Performance evaluation of hybrid GA–SVM and GWO–SVM models to predict earthquake-induced liquefaction potential of soil: A multi-dataset investigation. *Engineering with Computers, 38*(S5), 4197–4215. https://doi.org/10.1007/s00366-021-01418-3

Zhu, Z., & Zhang, Y. (2022). Flood disaster risk assessment based on random forest algorithm. *Neural Computing & Applications, 34*(5), 3443–3455. https://doi.org/10.1007/s00521-021-05757-6